The triple anomalous gauge couplings investigation on linear $e\gamma$-collider

I.A. Shershan* and T.V. Shishkina†
Department of Theoretical Physics and Astrophysics, Belarussian State University
Nezavisimosti Av. 4, 220006 Minsk, Belarus

The differential and total cross sections of the single gauge boson production in quasielastic high energy electron-photon scattering are obtained within the Standard Model in leading order and next-to-leading order of the perturbative theory. The contribution of divergent part of hard photon bremsstrahlung was included. The anomalous gauge boson coupling in the effective Lagrangian approach were studied. It is shown the analysis of neutral gauge couplings can be fully performed for two constants with different types of symmetries. Numerical analysis has been done. The best conditions were determined for registration of generated effects beyond the Standard Model.

PACS numbers: 12.15.Lk, 12.60.Cn, 14.60.Cd
Keywords: photon, electron, gauge boson, electroweak interaction, radiative corrections, linear colliders

I. INTRODUCTION

The Standard Model (SM) is the most advanced theory for describing the particles interactions. However, it is obvious that the SM is not the universal theory, but only a low-energy approximation of more extensive model. Nevertheless, new effects which allow to state the existence of the "new physics" (physics beyond the SM) have not been discovered. For this reason the most theoretical investigations are realized for the construction and study of various extended gauge models. As a rule, these models have a considerable simplicity and predictive power. The study of such models is the purpose of experiments on the linear accelerators of next generation.

The precision covariant calculation of the processes within the SM, taking into account radiation and polarization effects is important task also, because the "new physics" search should be obtained in comparison of theoretical and experimental data. Therefore, this investigation requires high accuracy of the experiments as well as the theoretical calculations. Numerical analysis must be performed with high precision.

The most promising models for the research on linear colliders are the models including anomalous triple and quartic gauge boson interactions. From the most general view, it is possible to construct a generalized Lagrangian for this kind of interaction, limiting consideration of operators of finite dimension. This approach is called the effective Lagrangian method, which includes not only the above mentioned operators, but also the new anomalous gauge coupling (AGC) [1, 2].

This paper is devoted to the study of the triple anomalous gauge couplings for $Z^*Z\gamma$, $\gamma^*Z\gamma$ and $W^*W\gamma$ anomalous interactions, which could be studied on the base of the processes of electron-photon interactions. These processes [3–6]

$$e^-\gamma \to e^-\gamma, \quad (1)$$
$$e^-\gamma \to e^-Z, \quad (2)$$
$$e^-\gamma \to \nu_e W^-, \quad (3)$$

can be investigated with the precise accuracy on linear accelerators of new generation, such as the International Linear Collider (ILC) [7, 8].

*Electronic address: shershan@bsu.by
†Electronic address: shishkina.tatiana.v@gmail.com

The study of processes with $e\gamma$ beams have a set of advantages. Collider luminosity in $e\gamma$-mode is extremely high. Even at the most possible interaction energy, cross sections of corresponding processes have magnitude about some picobarn. High energy photon beams can be obtained using Compton backscattering and this process can be separately studied. The process (3) has an exceptional importance in the triple AGC investigation, since it is the only one that allows to study pure $W^*W\gamma$ anomalous gauge interaction. It should be noted that on the base of the bremsstrahlung processes (from 2 to 3) is also possible to carry out the research of quartic anomalous gauge interactions including two real photons.

II. CROSS SECTIONS

A. Kinematic

We start from consideration of general process

$$\begin{aligned} e^-(p, m_e) + \gamma(k, 0) \to \\ \to C^-(p_1, m_c) + N^0(k_1, m_n), \end{aligned} \tag{4}$$

where C^- and N^0 are the final particles (charged and neutral); $p(p_1)$ and $k(k_1)$ are the 4-momenta of initial(final) charged and neutral particles, correspondingly; $m_e(m_c)$ and $0(m_n)$ are their masses. Corresponding Feynman diagrams for the general process of tree level are presented on Fig. 1.

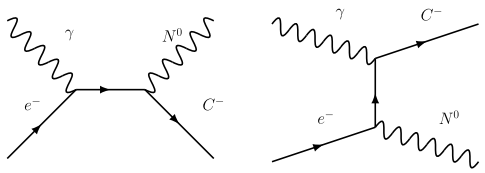

Figure 1: Feynman diagram for the $e^-\gamma \to C^-N^0$ process in the Born approximation

The expression of the total cross section for the such type of processes can be written as follows:

$$\sigma = \frac{1}{8\pi(s - m_e^2)^2} \int |\mathcal{M}|^2 \, dQ^2, \tag{5}$$

where s and t are Mandelstam variables:

$$s = (p + k)^2, \tag{6}$$

$$t \equiv -Q^2 = (p - p_1)^2, \tag{7}$$

and $\mathcal{M}$ is the process amplitude. Integration can be performed using the following limits:

$$Q^2_{\pm} = \frac{(s + m_e^2)(s + m_c^2 - m_n^2) \pm (s - m_e^2)\sqrt{\lambda(s, m_c^2, m_n^2)}}{2s} - m_c^2 - m_n^2. \tag{8}$$

B. Radiative corrections

1. One-loop contribution

Taking into account the one-loop radiative corrections, squared amplitude can be written as follows:

$$|\mathcal{M}|^2 = |\mathcal{M}_{born}|^2 + \Re|\mathcal{M}_{born} \cdot \mathcal{M}_V^*|, \tag{9}$$

where $\mathcal{M}_{born}$ is the Born approximation amplitude and $\mathcal{M}_V$ is the amplitude including virtual radiative corrections (RC).

One-loop corrections contain unphysical ultraviolet (UV) and infrared (IR) divergences. This divergences must be regularized. Usually, the dimensional regularization is chosen for this purpose, which allows one to parameterize both types of divergences by performing integration in N-dimensional space [9]. UV-divergencies can be reduced by summation with additional counter-term diagrams contribution. Counter-terms choose in accordance with

corresponding renormalization scheme. In this paper on-mass shell renormalization scheme was chosen. Finally, the amplitude of virtual radiative corrections can be written as follows:

$$\mathcal{M}_V = \mathcal{M}_{OL} + \mathcal{M}_{CT}, \tag{10}$$

where $\mathcal{M}_{OL}$ is the one-loop contribution amplitude and $\mathcal{M}_{CT}$ is the counter-terms contribution amplitude.

2. Soft photon contribution

Cancellation of IR-divergences is performed by taking into account the soft photon bremsstrahlung contribution. In this case the differential cross section level can be written as

$$d\sigma_{soft} = \delta_{soft} \cdot d\sigma_{born}. \tag{11}$$

Here factor δ_{soft} is calculated as follows:

$$\delta_{soft} = -\frac{\alpha}{2\pi^2} \int_0^{\Delta E} \left[\frac{p^2}{(2pq)^2} + \frac{p_1^2}{(2p_1q)^2} - \frac{2pp_1}{(2pq)(2p_1q)} \right], \tag{12}$$

where α is fine structure constant and ΔE is the collider energy resolution. This energy is the minimal energy of the final bremsstrahlung photon that can be detected.

Performing integration in accordance with the dimensional regularization scheme for each of the terms in brackets, the factor δ_{soft} can be rewritten:

$$\delta_{soft} = -\frac{\alpha}{2\pi^2} \int_0^{\Delta E} \left[I(p) + I(p_1) - I(p, p_1) \right]. \tag{13}$$

The functions $I(q)$, $I(q_i, q_j)$ can be presented in the form [10, 11]:

$$I(q) = \pi \left[-\Delta^{IR} + \log \frac{4\Delta E^2}{\mu^2} + \frac{q^0}{|\vec{q}|} \log \frac{q^0 - |\vec{q}|}{q^0 + |\vec{q}|} \right], \tag{14}$$

$$I(q_i, q_j) = 2\pi \frac{\zeta^2 x_{ij}}{\zeta^2 m_i^2 - m_j^2} \left[\frac{1}{2} \log \frac{\zeta^2 m_i^2}{m_j^2} \left(-\Delta^{IR} + \log \frac{4\Delta E^2}{\mu^2} \right) + \right. \tag{15}$$

$$\left. + \left\langle \frac{1}{2} \log^2 \frac{u^0 - |\vec{u}|}{u^0 + |\vec{u}|} + \mathrm{Li}_2 \left(1 - \frac{u^0 + |\vec{u}|}{v} \right) + \mathrm{Li}_2 \left(1 - \frac{u^0 - |\vec{u}|}{v} \right) \right\rangle_{u=q_j}^{u=\zeta q_i} \right], \tag{16}$$

where μ is t'Hoft-Veltman mass parameter and

$$\zeta = \frac{x_{ij} + \sqrt{x_{ij}^2 - 4m_i^2 m_j^2}}{2m_i^2},$$

$$v = \frac{\zeta^2 m_i^2 - m_j^2}{2(\zeta q_i^0 - q_j^0)},$$

$$x_{ij} = 2q_i \cdot q_j.$$

In the case of the process (4) one can obtain

$$p^0 = \frac{s+m_e^2}{2\sqrt{s}}, p_1^0 = \frac{s+m_c^2}{2\sqrt{s}},$$
$$|\vec{p}| = \frac{s-m_e^2}{2\sqrt{s}}, |\vec{p_1}| = \frac{s-m_c^2}{2\sqrt{s}},$$
$$x_{ij} = Q^2 + m_e^2 + m_c^2.$$

3. Hard photon contribution

The soft photon bremsstrahlung contribution depends on the collider energy resolution. However, in the soft photon approximation this energy should be much less than the interaction energy (including the masses of particles). In the present experiments, it is impossible to achieve such precision. To avoid this dependence one can take into account the hard photon bremsstrahlung contribution. The process (4) with additional final real photon can be rewritten as follows:

$$e^-(p, m_e) + \gamma(k, 0) \to$$
$$\to C^-(p_1, m_c) + N^0(k_1, m_n) + \gamma(q, 0).$$

The expression of the total cross section for the such type of processes has the following form:

$$\sigma = \frac{(2\pi)^{-4}}{4(s-m_e^2)^2} \int |\mathcal{M}_{hard}|^2 \times \frac{dt_1 ds_1 ds_2 dt_2}{8\sqrt{-\Delta_4}}, \quad (17)$$

where s, t_1, s_1, s_2, t_2 are Mandelstam variables:

$$s = (p+k)^2,$$
$$t_1 = (k-k_1)^2,$$
$$s_1 = (p_1+q)^2;$$
$$s_2 = (p_1+k_1)^2;$$
$$t_2 = (p-q)^2.$$

The part corresponding to the localization of IR-divergence is the main contribution to the cross section of the bremsstrahlung process. Therefore, one can divide $\mathcal{M}_{hard}|^2$ into the divergent and finite parts:

$$|\mathcal{M}_{hard}|^2 = |\mathcal{M}_{hard}^{IR}|^2 + \text{finite part}. \quad (18)$$

It is very useful, because $|\mathcal{M}_{hard}|^2$ can be factorized by squared matrix element in the Born approximation:

$$|\mathcal{M}_{hard}|^2 = \delta_{hard}^{IR} |\mathcal{M}_{born}|^2. \quad (19)$$

Factor δ_{hard}^{IR} depends on all new invariant and can be expressed as follows:

$$\delta_{hard}^{IR} = -\frac{\alpha}{\pi^2} \int \left(\frac{m_e^2}{(m_e^2 - t_2)^2} + \frac{m_c^2}{(s_1 - m_c^2)^2} - \frac{Q^2 + m_e^2 + m_c^2}{(m_e^2 - t_2)(s_1 - m_c^2)} \right) \quad (20)$$

where Δ_4 is the Gram determinant

$$\Delta_4 = \begin{vmatrix} p^2 & (pk) & (pp_1) & (pk_1) \\ (kp) & k^2 & (kp_1) & (kk_1) \\ (p_1p) & (p_1k) & p_1^2 & (p_1k_1) \\ (k_1p) & (k_1k) & (k_1p_1) & k_1^2 \end{vmatrix}. \quad (21)$$

All kinematic boundaries can be obtained from the condition $\Delta_4 = 0$.

After the integration over s_2, s_1, t_2 the invariant t_1 can be identified with t. Finally, for δ_{hard}^{IR} one can obtain [12]

$$\delta^{IR}_{hard} = -\frac{\alpha}{2\pi}\left\langle \log\frac{4\Delta E^2 m_c^2}{(\bar{s}_1 - m_c^2)^2}\left[2 - \frac{1}{\beta_t}\log x_t\right] + \Re\left\{\log s_1 - 2\log\frac{m_c^2 - t}{s_1 - t} - \right.\right.$$
$$- \log^2(s_1 - t) + \log(\bar{s}_1 - m_c^2)(2\log(s_1 - t) - \log m_e^2 s_1) + \quad (22)$$
$$\left.\left. + \log m_e^2 s_1 \log\frac{m_c^2(s_1 - t)}{-t} - \mathrm{Li}_2\frac{s_1}{m_c^2} + \mathrm{Li}_2\frac{s_1}{t} + 2\mathrm{Li}_2\frac{s_1 - t}{m_c^2 - t}\right\}^{s_1=\bar{s}_1}_{s_1=m_c^2}\right\rangle$$

with

$$\beta_t = \frac{\sqrt{\lambda(t, m_e^2, m_c^2)}}{m_e^2 + m_c^2 - t}, \quad (23)$$
$$x_t = \frac{1+\beta_t}{1-\beta_t}. \quad (24)$$

Summarizing of all above mentioned, one can write the expression for the differential cross section, including the lowest-order radiative corrections:

$$d\sigma = d\sigma_{born}(1 + \delta^{IR}_{soft} + \delta^{IR}_{hard}) + d\sigma_V, \quad (25)$$

and introduce the general notation for full relative radiative corrections

$$\delta^{full} = (d\sigma/d\sigma_{born} - 1) \times 100\% \quad (26)$$

or

$$\delta^{full} = (\sigma/\sigma_{born} - 1) \times 100\% \quad (27)$$

in case of the total cross sections.

C. Anomalous gauge couplings

Effective lagrangian of anomalous $WW\gamma$ interaction can be presented in following form [13]:

$$-\mathcal{L}_{WW\gamma}/e = i\kappa_\gamma W^\dagger_\mu W_\nu F^{\mu\nu} +$$
$$+\frac{i\lambda_\gamma}{m_W^2} W^\dagger_{\lambda\mu} W^\mu{}_\nu F^{\nu\lambda} - g_4^\gamma W^\dagger_\mu W_\nu \left(\partial^\mu A^\nu + \partial^\nu A^\mu\right) +$$
$$+ g_5^\gamma \varepsilon^{\mu\nu\rho\sigma}\left(W^\dagger_\mu \overleftrightarrow{\partial}_\rho W_\nu\right) A_\sigma + i\tilde{\kappa}_\gamma W^\dagger_\mu W_\nu \tilde{F}^{\mu\nu} + \frac{i\tilde{\lambda}_\gamma}{m_W^2} W^\dagger_{\lambda\mu} W^\mu{}_\nu \tilde{F}^{\nu\lambda}, \quad (28)$$

where F_μ is electromagnetic field tensor, W_μ is W-boson field, $W_{\mu\nu} = \partial_\mu W_\nu - \partial_\nu W_\mu$, $V_{\mu\nu} = \partial_\mu V_\nu - \partial_\nu V_\mu$, $\tilde{V}_{\mu\nu} = \frac{1}{2}\varepsilon_{\mu\nu\rho\sigma}V^{\rho\sigma}$, $(A \overleftrightarrow{\partial}_\mu B) = A(\partial_\mu B) - B(\partial_\mu A)$.

Following eq. (28) one can put a vertex function of the form

$$\Gamma_{\gamma}^{\alpha\beta\mu}(q,\overline{q},P) = \frac{\lambda_\gamma}{m_W^2}\left(q_\nu g^{\rho\alpha} - q^\rho g_\nu^\alpha\right)\left(\overline{q}_\rho g_\sigma^\beta - \overline{q}_\sigma g_\rho^\beta\right)\left(P^\sigma g^{\mu\nu} - P^\nu g^{\mu\sigma}\right) + \\ + \frac{\tilde{\lambda}_\gamma}{2m_W^2}\left(q_\nu g^{\rho\alpha} - q^\rho g_\nu^\alpha\right)\left(\overline{q}_\rho g_\sigma^\beta - \overline{q}_\sigma g_\rho^\beta\right)\left(P_\gamma g_\tau^\mu - P^\tau g_\gamma^\mu\right)\varepsilon^{\sigma\nu\gamma\tau} - \\ - \Delta\kappa_\gamma\left(P^\alpha g^{\beta\mu} - P^\beta g^{\alpha\mu}\right) + \tilde{\kappa}_\gamma \varepsilon^{\alpha\beta\mu\nu}P_\nu \qquad (29)$$

with CP-odd $(\lambda_\gamma,\, \delta\kappa_\gamma)$ and CP-even $(\tilde{\kappa}_\gamma,\, \tilde{\lambda}_\gamma)$ AGC. In similar way vertex function of $V^*Z\gamma$ interaction can be presented as

$$\Gamma_{ZV\gamma}^{\alpha\beta\mu}(q_1,q_2,P) = \frac{s-m_V^2}{m_Z^2}\left[h_1^V\left(q_2^\mu g^{\alpha\beta} - q_2^\alpha g^{\mu\beta}\right) + \frac{h_2^V}{m_Z^2}P^\alpha\left(P\cdot q_2 g^{\mu\beta} - q_2^\mu P^\beta\right) + \right. \\ \left. + h_3^V\varepsilon^{\mu\alpha\beta\rho}q_{2\rho} + \frac{h_4^V}{m_Z^2}P^\alpha\varepsilon^{\mu\beta\rho\sigma}P_\rho q_{2\sigma}\right]. \qquad (30)$$

The couplings h_1^V and h_2^V are P-odd, h_3^V and h_3^V are P-even, all couplings are C-odd.

III. NUMERICAL ANALYSIS

To carry out numerical analysis, some software is required. The presented results were obtained using the following tools:

- Analytical results: ***Wolfram Mathematica*** system [14];
- Squared matrix elements: ***FormCalc*** package;
- Processes kinematics: ***FeynCalc*** package [15];
- Passarino-Veltman integration: ***LoopTools*** library [16];
- Numerical integration: ***Vegas*** Monte-Carlo simulator [17].

The parametrization of unphysical UV- and IR-divergencies were performed using dimensional regularization. Final results do not depend on t'Hoft-Veltman mass regulator μ^2 and collider energy resolution ΔE. On-mass shell regularization scheme was choosed. Following experimental features were used: scattered particle angle cut $\Delta\vartheta = 20^\circ$, ΔE is varied in the wide range of values to confirm the independence of final results from this parameter. Since the search for "new physics" implies a set of impressive experimental statistics, the analysis of the possible contribution of anomalous interactions was carried out on the basis of the total cross sections. Anomalous gauge couplings constraints were determined taking into account the following value for standard deviation σ^{SD}:

$$\sigma^{SD} = 0.001\cdot\sigma(s_0) + 1/\mathfrak{L}_{\text{int}}$$

with integrated luminosity $\mathfrak{L}_{\text{int}} = 100\ \text{pb}^{-1}$. Anomalous interactions study was performed using ND-fit. It means that only N AGC is free and other one have there SM values.

A. Standard Model results

The relative radiative corrections to differential cross section for all processes with different interaction energies are shown in

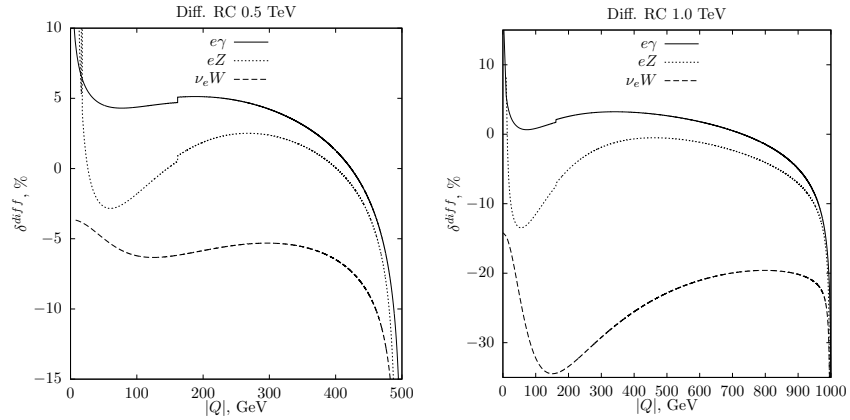

Figure 2: The differential radiative corrections for a set of processes.

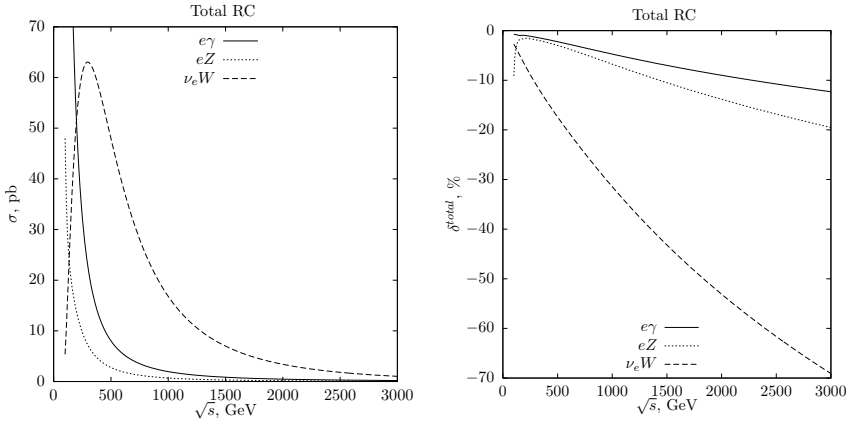

a) b)

Figure 3: The total cross sections including the lowest order radiative corrections a) and relative radiative corrections b) for a set of processes.

Fig. 2. As one can see, RC to differential cross section strongly depends on interaction energy and they absolute value principally increase with energy growth. For the all considered processes, a characteristic feature is the kinks and corresponding local extrema in the regions of the minimum and maximum values of the momentum transfer module $|Q|$. At $\sqrt{s}$=1.0 TeV typical values of relative RC to differential cross section for the Compton scattering process and Z-boson production process are within the range of $-12 \div 0\%$, for the W-boson production process within the range of $-35 \div -13\%$.

The total cross sections including RC and relative RC for all processes under consideration are shown in Fig. 3. With increasing of interaction energy, the absolute values of the cross sections decreases for all processes. In case of W-boson production cross section has a peak with value about 64 pb at interaction energy $\sqrt{s}$=310 GeV. At $\sqrt{s}$=1.5 TeV cross sections of all processes don't exceed 10 pb. RC have principally negative values. It is reach -38% for the W-boson production process and interaction energy $\sqrt{s}$=1 TeV. This behavior is explained by the absence of the bremsstrahlung contribution, which is not related to the presence of IR-divergences in the current calculations. Consideration of finite hard bremsstrahlung contribution for this process is very important. RC do not exceed -10% for the processes of neutral gauge bosons production at the same interaction energy.

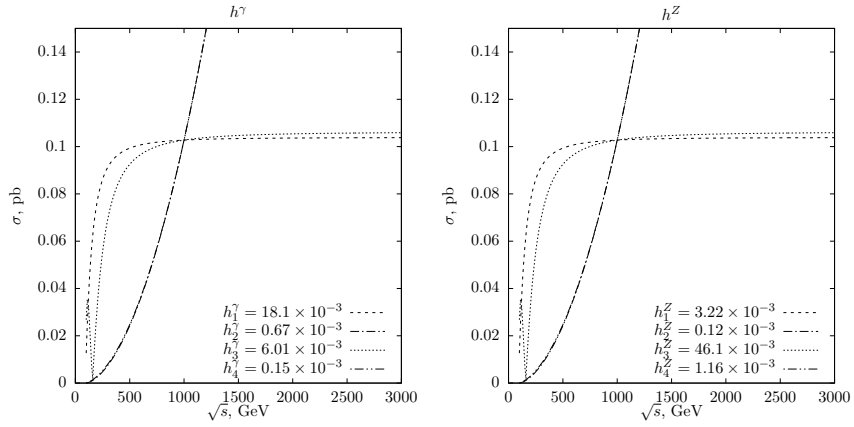

Figure 4: The total cross section of $e\gamma \to eZ$ process obtained using $1\sigma^{SD}$ limits for h_i^γ and h_i^Z

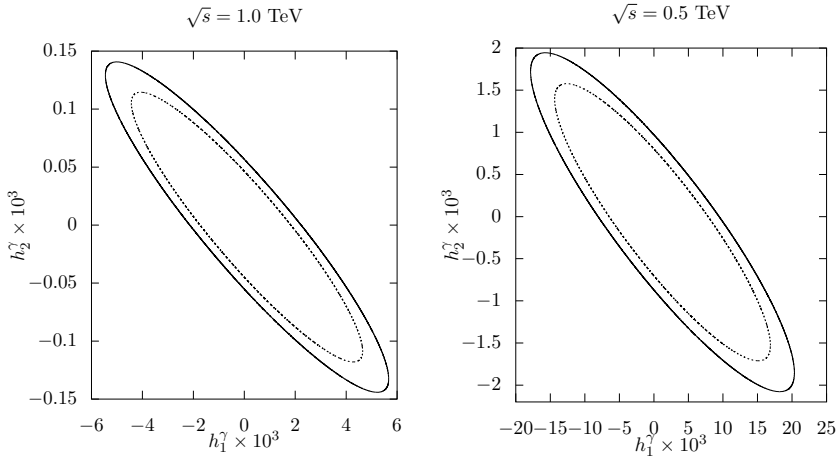

Figure 5: 99% (solid lines) and 95% (dashed lines) C.L. constraints for the $(h_1^\gamma,\, h_2^\gamma)$ gauge couplings

B. $V^*Z\gamma$ interactions

We start from the analysis of anomalous $V^*Z\gamma$ interactions behavior. In the linear approximation anomalous contribution to the total cross section of Z-boson production can be written in the following form:

$$\sigma_{eZ}^{(1)} = \sum_{i,V} h_i^V \cdot f_i^V, \qquad (31)$$

where f_i^V are form-factors of corresponding AGC. In 1D-fit constraints can be derived with 68% confidence level (C.L.) from the following inequality:

$$\sigma^{SD} \geq |h_i^V \cdot f_i^V| \qquad (32)$$

Contributions of terms for every $V^*Z\gamma$ coupling in 1D-fit are presented in Fig. 4. As one can see, with increasing of interaction energy the absolute value of couplings with odd indexes increases fast starting from energy value about 1.5 TeV. This behavior is explained by the presence of a gauge cancellation. The extremely important result of this analysis is that contributions of CP-odd/even couplings to the $e\gamma \to eZ$ process are indistinguishable, both qualitatively and quantitatively. This fact suggests that the 2D-fit analysis for the $(h_1^\gamma,\, h_2^\gamma)$ will be sufficient for a complete analysis of neutral AGC.

2D-fit is based on the quadratic polynom. $N\sigma^{SD}$ neutral AGC constrains have been derived from the following inequality:

$$N\sigma^{SD} \geq |\sigma_{eZ}^{(1)} + \sigma_{eZ}^{(2)}|, \qquad (33)$$

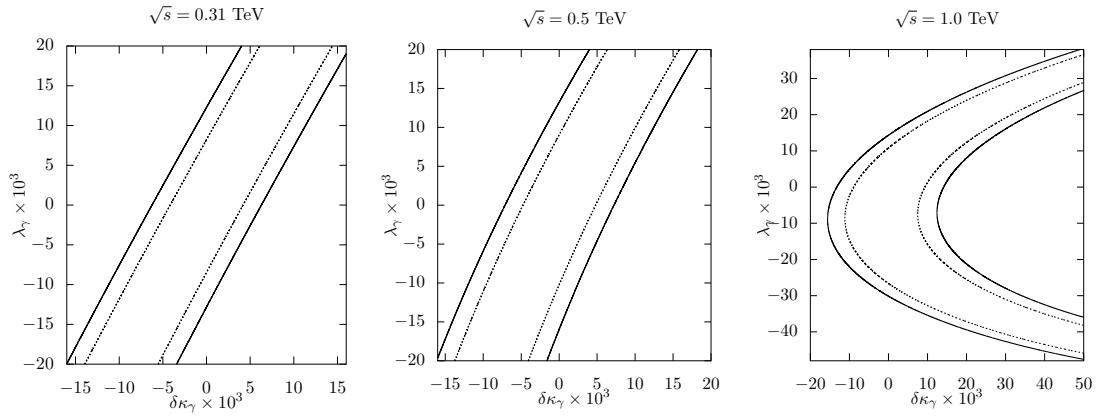

Figure 6: 99% (solid lines) and 95% (dashed lines) C.L. constraints for the ($\delta\kappa_\gamma$, λ_γ) gauge couplings

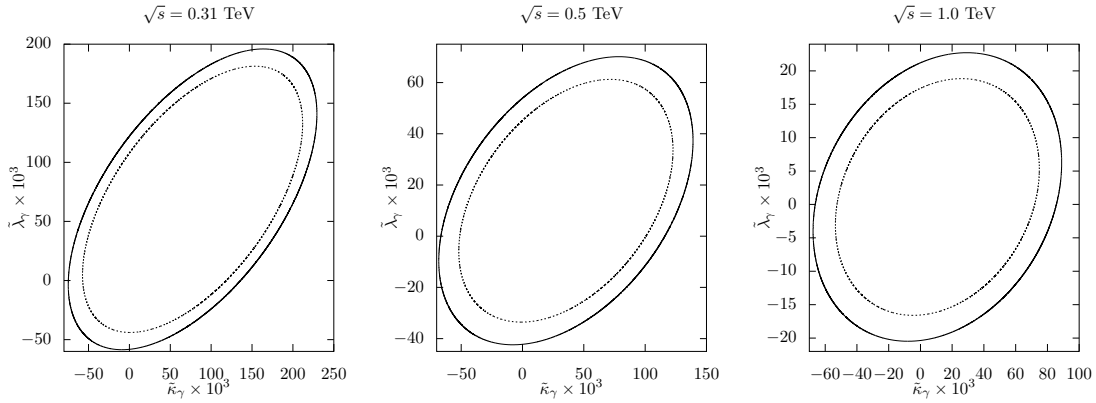

Figure 7: 99% (solid lines) and 95% (dashed lines) C.L. constraints for the $\left(\tilde{\kappa}_\gamma, \tilde{\lambda}_\gamma\right)$ gauge couplings

where

$$\sigma_{eZ}^{(2)} = \sum_{i,j} h_i^\gamma h_j^\gamma \cdot g_{ij}. \qquad (34)$$

Results of 2D-fit of 2σ and 3σ levels for different interaction energies are presented in Fig. 5. In the case of 2D-fit, the constraints are much tougher. With an increasing of the interaction energy, the obtained restrictions strongly growth. Therefore, the research of neutral AGC seems to be the most promising at the highest possible energies.

C. $W^*W\gamma$ interactions

2D-fit analysis of CP-odd/even charged AGC has been performed separately and is based on eq. 33. Restrictions on the CP-odd couplings ($\delta\kappa_\gamma$, λ_γ) depending on different interaction energies can be found in Fig. 6.

As one can see, the range of possible AGC is a ring, which size decreases with increasing $\sqrt{s}$. Constraints are defined in the range near the SM values. If one compares the regions for different energy values, it will give further limit of the range of AGC.

Restrictions on the CP-even couplings $\left(\tilde{\kappa}_\gamma, \tilde{\lambda}_\gamma\right)$ depending on different interaction energies are presented in Fig. 7. It is easy to see that in this case, as the energy increases, it is possible to significantly refine the restrictions on the anomalous coupling constants. This behavior indicates the potential benefits of increasing the design capability of the next-generation accelerators.

The possible behavior of the anomalous contributions to the cross sections of the processes at AGC values at the boundary of the $3\sigma^{SD}$ regions of 2D-fits is shown in

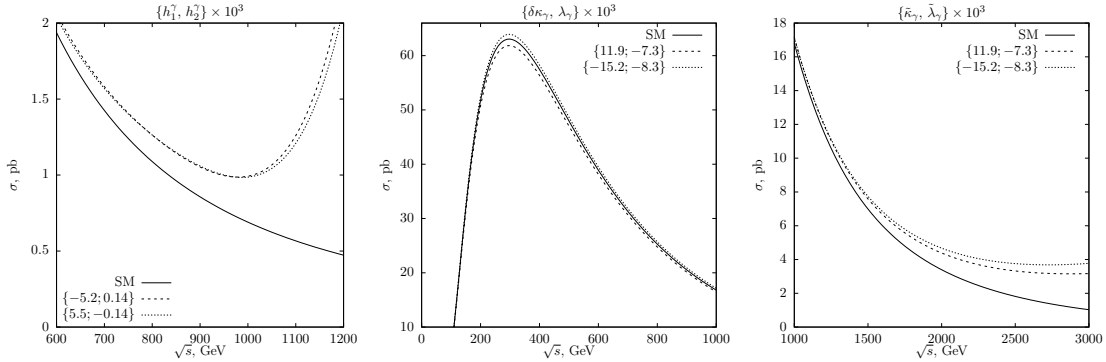

Figure 8: Results for some $3\sigma^{SD}$ boundary values of different anomalous gauge couplings

AGC	LEP	ILC 0.31 TeV	ILC 0.5 TeV	ILC 1.0 TeV
$h_1^\gamma \times 10^3$	[-50, 50]	—	[-18.06, 19.10]	[-17.70, 17.70]
$h_2^\gamma \times 10^3$	[-40, 20]	—	[-0.671, 0.671]	[-0.658, 0.658]
$h_3^\gamma \times 10^3$	[-50, 0]	—	[-6.009, 6.009]	[-5.887, 5.887]
$h_4^\gamma \times 10^3$	[10, 50]	—	[-0.151, 0.151]	[-0.148, 0.148]
$h_1^Z \times 10^3$	[-120, 110]	—	[-3.222, 3.222]	[-3.157, 3.157]
$h_2^Z \times 10^3$	[-70, 70]	—	[-0.120, 0.120]	[-0.117, 0.117]
$h_3^Z \times 10^3$	[-190, 60]	—	[-46.13, 46.13]	[-45.20, 45.20]
$h_4^Z \times 10^3$	[-40, 130]	—	[-1.160, 1.160]	[-1.137, 1.137]
$h_1^\gamma \times 10^3$	[-50, 50]	—	[-17.82, 20.26]	[-5.467, 5.663]
$h_2^\gamma \times 10^3$	[-40, 20]	—	[-2.072, 1.949]	[-0.144, 0.140]
$\delta\kappa_\gamma \times 10^3$	[-99, 66]	[-6.242, 6.290]	[-7.125, 7.221]	[-15.85, 12.25]
$\lambda_\gamma \times 10^3$	[-59, 17]	[-12.82, 12.27]	[-15.95, 13.24]	[-36.41, 22.19]
$\tilde{\kappa}_\gamma \times 10^3$	—	[-75.63, 229.0]	[68.56, 138.7]	[-67.75, 88.66]
$\tilde{\lambda}_\gamma \times 10^3$	—	[-58.47, 195.7]	[-41.92, 70.18]	[-20.46, 22.76]

Table I: 95% C.L. anomalous gauge couplings limits and LEP experimental data [18]

Fig. 8. Obviously, in the most cases, the search for AGC should be performed at the maximum possible particle interaction energies. For the ($\delta\kappa_\gamma$, λ_γ) pair of couplings, the best region for searching of deviations from the SM will be the region near the peak of the W-boson production.

IV. CONCLUSION

In the paper the differential and total cross sections of the gauge bosons production processes in electron-photon collisions including radiative corrections were calculated. As it was shown by numerical analysis, the contribution of radiative corrections is significant and this strongly affect on the background. The hard bremsstrahlung contribution was made taking into account only the IR-divergent part. It demonstrates the good results for the production of neutral gauge bosons. For the calculation of W-boson production process the IR-finite contribution is needed, because it has significant value in cross section of the process near the W-boson production peak. Consideration of the finite bremsstrahlung contribution seems a logical continuation of research.

Anomalous gauge boson interactions were studied. Final results are presented in Tab. I. As one can see the large integral luminosity will be able significantly clarify the constraints for AGC on ILC. The numerical analysis shows that the search for manifestations of ($\delta\kappa_\gamma$, λ_γ) is the best near the peak of the W-boson production. This is be-

cause the operators corresponding to these constants are 4D. Another AGC contributions set by 6D operators are significant on maximal possible interaction energy. For the $e\gamma \to eZ$ process the analysis can be performed using 2D-fit only for pair of couplings with different CP-symmetry.

[1] H. Aihara, T. Barklow, U. Baur, J. Busenitz, S. Errede, T. Fuess, T. Han, D. London, J. Ohnemus, R. Szalapski, et al., in *Electroweak symmetry breaking and new physics at the TeV scale* (World Scientific, 1996), pp. 488–547.

[2] T. Barklow, U. Baur, F. Cuypers, S. Dawson, D. Errede, S. Errede, S. Godfrey, T. Han, P. Kalyniak, K. Riles, et al., arXiv preprint hep-ph/9611454 (1996).

[3] A. Denner and S. Dittmaier, Nuclear Physics B **540**, 58 (1999).

[4] A. Denner and S. Dittmaier, Nuclear physics B **398**, 265 (1993).

[5] M. Böhm and S. Dittmaier, Nuclear Physics B **409**, 3 (1993).

[6] T. Shishkina, Nonliner phenomena in complex systems **11**, 60 (2011).

[7] T. Behnke, J. E. Brau, B. Foster, J. Fuster, M. Harrison, J. M. Paterson, M. Peskin, M. Stanitzki, N. Walker, and H. Yamamoto, arXiv preprint arXiv:1306.6327 (2013).

[8] I. Ginzburg, G. Kotkin, S. Panfil, V. Serbo, and V. I. Telnov, Nuclear Instruments and Methods in Physics Research **219**, 5 (1984).

[9] G. Passarino and M. Veltman, Nuclear Physics B **160**, 151 (1979).

[10] G. t Hooft and M. Veltman, Nuclear Physics B **153**, 365 (1979).

[11] A. Akhundov, D. Bardin, L. Kalinovskaya, and T. Riemnann, Fortschritte der Physik **44**, 373 (1996).

[12] D. Y. Bardin, Nucl. Phys. **127**, 242 (1977).

[13] K. Hagiwara, R. Peccei, D. Zeppenfeld, and K. Hikasa, Nuclear Physics B **282**, 253 (1987).

[14] S. Wolfram, *Mathematica: A System for Doing Mathematics by Computer: User's Guide for Microsoft Windows* (Addison-Wesley, 1992).

[15] R. Mertig, M. Böhm, and A. Denner, Computer Physics Communications **64**, 345 (1991).

[16] T. Hahn, Nuclear Physics B-Proceedings Supplements **89**, 231 (2000).

[17] G. P. Lepage, Journal of Computational Physics **27**, 192 (1978).

[18] A. Collaboration, D. collaboration, L. Collaboration, O. Collaboration, L. E. W. Group, et al., Physics reports **532**, 119 (2013).